LA-UR-15-27996
Approved for public release; distribution is unlimited.

Title: Density functional theory calculations of defect and fission gas properties in U-Si fuels

Author(s): Andersson, Anders David Ragnar

Intended for: Report

Issued: 2016-02-03 (rev.1)

# Density functional theory calculations of defect and fission gas properties in U-Si fuels

David Andersson

Los Alamos National Laboratory, Los Alamos, New Mexico 87545, USA

## Introduction

Accident tolerant fuels (ATF) are being developed in response to the Fukushima Daiichi accident in Japan. One of the options being pursued is U-Si fuels, such as the $U_3Si_2$ and $U_3Si_5$ compounds, which benefit from high thermal conductivity (metallic) compared to the $UO_2$ fuel (insulator or semi-conductor) used in current Light Water Reactors (LWRs). The U-Si fuels also have higher fissile density. In order to perform meaningful engineering scale nuclear fuel performance simulations, the material properties of the fuel, including the response to irradiation environments, must be known. Unfortunately, the data available for U-Si fuels are rather limited, in particular for the temperature range where LWRs would operate. The ATF HIP is using multi-scale modeling and simulations to address this knowledge gap.

The present study investigates point defect and fission gas properties in $U_3Si_2$, which is one of the main fuel candidates, using density functional theory (DFT) calculations. Based on a few assumption regarding entropy contributions, defect and fission diffusivities are predicted. Even though uranium silicides have been shown to amorphize easily at low temperature, we assume that $U_3Si_2$ remains crystalline under the conditions expected in Light Water Reactors (LWRs). The temperature and dose where amorphization occurs has not yet been well established.

## Methodology

The DFT calculations were carried out with the VASP code [1-3] using the projector augmented-wave (PAW) method and Perdew-Burke-Ernzerhof (PBE) [7] potentials for the exchange-correlation potentials. This methodology has been shown to work well for the U and Si end-member systems. However, initial calculations showed that the $U_3Si_2$ crystal structure (Figure 1) is not stable within the PBE method. This is not obvious from calculations on the unit cell in Figure 1 (i.e. the unit cell structure does not spontaneously transform), but phonon calculations give negative frequencies and calculations on the 2×2×2 supercell relaxes to a distorted structure with much lower energy (0.10 eV/atom). The new relaxed structure is shown in Figure 2. There is, however, no experimental support for breaking the symmetry of the $U_3Si_2$ crystal structure (space group P4/mbm), which suggests that the DFT calculations fail to capture some important physics. The most obvious suspect is the U 5f electrons, which are known to exhibit strong correlation effects. There are several ways to describe the strongly correlated properties of the U 5f electrons, such as the Hubbard *U* method, hybrid functionals and dynamical mean field theory (DMFT). Here we have applied the Hubbard *U* (PBE+*U*) method [8] due to its simplicity and computational efficiency, which allow us to study, for example, defect and fission gas

properties. The value of the *U* parameter is not known *a priori*. We tested several different *U* values ranging from 0 to 3 eV. For values of 1.5 eV or higher the distorted structure is no longer stable and relaxes back to the experimental structure with the space group P4/mbm. The application of the Hubbard *U* increases the unit cell volume slightly. We tried to artificially increase the $U_3Si_2$ volume within the PBE approach (no Hubbard *U*) to see if the stability is linked to the volume increase, but the distorted structure was still found to be more stable than the experimental crystal structure. The best balance between stability and volume is achieved for *U*=1.5 eV, which is henceforth used in this study. The stability of the $U_3Si_2$ structure seems to be related to splitting or localizing the *U* 5f electrons for *U* > 1.5 eV, as illustrated in Figure 3. The unit cell volume and formation energy of the $U_3Si_2$ structure are compared to experimental data in Table 1. The formation energy was calculated with respect to silicon in the diamond structure and α uranium. The unary α uranium structure did not apply the Hubbard *U* methodology, because its properties are better captured with the regular PBE potential, as is often the case for pure metals. In order to compare energies for α uranium without a Hubbard *U* parameter for the U 5f electrons and $U_3Si_2$ for which the U 5f electrons were modeled with a Hubbard *U* parameter, we relied on the methodology developed by Jain et al. [9]. USi in the FeB structure was used as the reference phase for calibration of the energy relating the electrons described with and without the Hubbard *U* parameter. Alternatively, the formation energy can be calculated with respect to α uranium applying the Hubbard *U* method for the U 5f electrons. For comparison, Table 1 includes the formation energy calculated using PBE alone, PBE+*U* using the approach in Ref. [9] to relate the U 5f electrons described with and without the Hubbard *U* model and PBE+*U* for both the $U_3Si_2$ and α uranium phases.

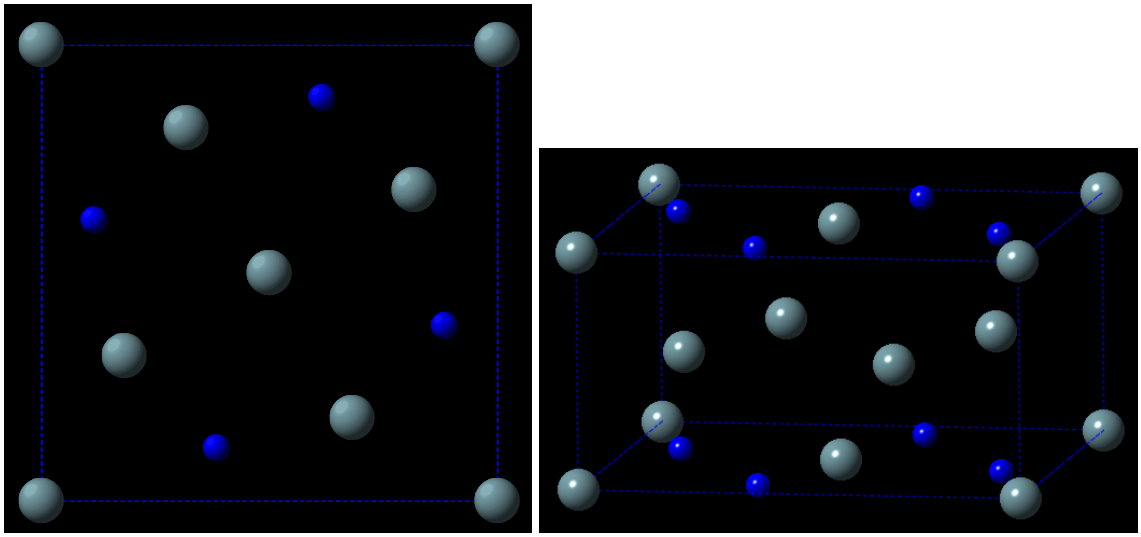

**Figure 1: The ideal $U_3Si_2$ unit cell viewed in the a-b plane (left) and tilted along the c axis (right). There are two U sites. We refer to the (0,0,0) and (0.5,0.5,0.5) sites as type 1 and the other sites as type 2.**

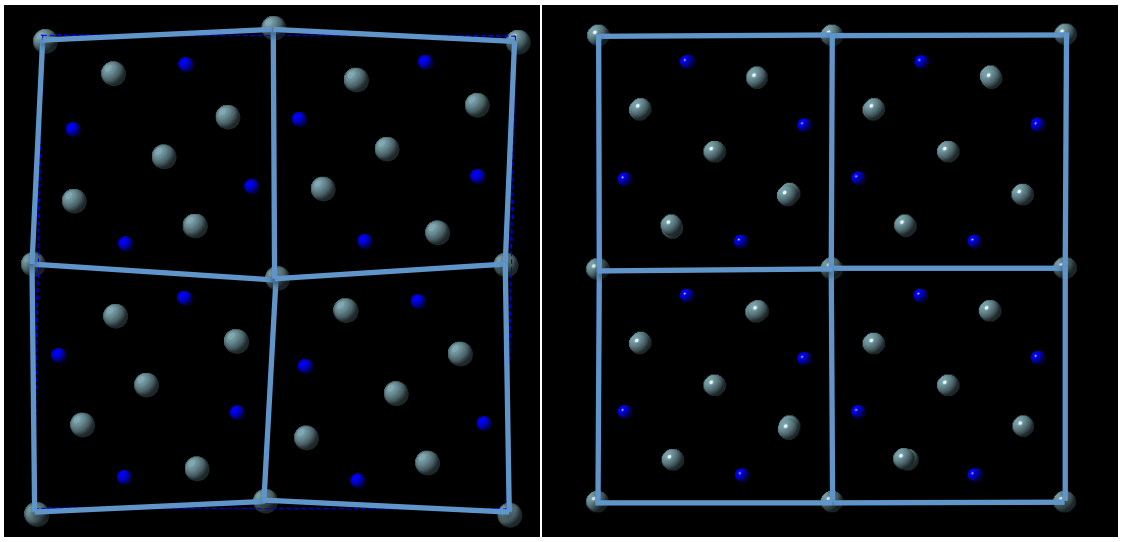

**Figure 2: The relaxed structure of the 2×2×2 $U_3Si_2$ supercell (left). The ideal 2×2×2 $U_3Si_2$ supercell (right). The PBE method predicts the relaxed structure to have much lower energy than the ideal structure (0.10 eV/atom).**

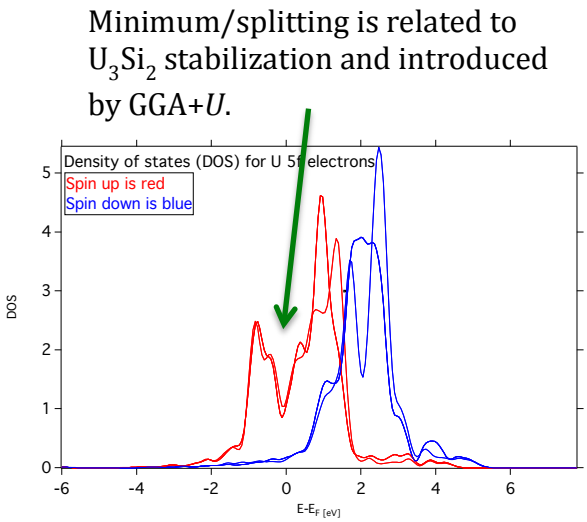


**Figure 3: The stability of the $U_3Si_2$ structure seems to be related to splitting or localizing the U-5f electrons for $U$ > 1.5 eV.**

**Table 1: Calculated and experimental volume and formation energy for $U_3Si_2$. Calc. PBE, PBE+$U$ or PBE+$U$* indicate that the reference energy for α uranium was calculated using the PBE, PBE+$U$ or PBE methodology plus the correction calculated according to the scheme developed by Jain et al [9]. See text for details.**

| $U_3Si_2$ | Volume (Å$^3$/atom) | Formation energy (eV/atom) |
|---|---|---|
| Calc. PBE | 20.47 | -0.15 |
| Calc. PBE+$U$ | 22.24 | -0.45 |
| Calc. PBE+$U$* | 22.24 | -0.37 |
| Exp. | 20.96 | -0.36 |

Defect properties were calculated in a 2×2×2 supercell expansion of the $U_3Si_2$ unit cell. Integration in reciprocal space was performed on either 2×2×2 or 4×4×4

Monkhorst-Pack k-point meshes. The plane-wave cut off energy was set to 500 eV and the partial occupancies were smeared according to the Methfessel-Paxton method with smearing width of 0.1 eV. Atomic positions, supercell volume and supercell shape was allowed to fully relax in all calculations (zero pressure and zero forces on the ions). All point defect energies were calculated with the chemical potentials defined by Si in the diamond structure and α uranium. The approach due to Jain et al. was used to relate the metallic α uranium reference state to $U_3Si_2$ and the $U_3Si_2$ supercell containing defects.

# Results

## Point defect formation energies

The point defect formation energies are summarized in Table 2. In addition to individual point defects, the Frenkel and Schottky defect reaction energies are included. Even though we will not present all the structural information in this report, it is worthwhile noting that the lowest energy U interstitial forms a split structure with one of the lattice U atoms. The negative formation energy of Si interstitials (with respect to silicon in the diamond structure) is consistent with the phase diagram and the slope of the convex hull. According to our results formation of vacancies preferably occurs by Frenkel reactions.

**Table 2: Calculated point defect formation energies as well as Frenkel and Schottky defect reaction energies.**

| Defect or reaction type | Energy (eV) |
|---|---|
| Uranium vacancy 1 | 1.64 |
| Uranium vacancy 2 | 2.65 |
| Si vacancy 1 | 2.48 |
| U interstitial 1 | 1.66 |
| U interstitial 2 | 0.65 |
| U interstitial 3 | 1.17 |
| Si interstitial 1 | 0.10 |
| Si interstitial 2 | 0.85 |
| Si interstitial 3 | -0.20 |
| U anti-site 1 | 1.70 |
| U anti-site 2 | 1.61 |
| Si anti-site 1 | 0.20 |
| Si anti-site 2 | 1.21 |
| U Frenkel reaction | 2.29 |
| Si Frenkel reaction energy | 2.28 |
| Schottky reaction energy | 10.08 |
| Bound Schottky defect | 7.71 |

## Xe trap site formation, incorporation and solution energies

In order to investigate fission gas diffusion and release, the probability of Xe (the most important fission gas) atoms occupying different lattice positions must be

determined, which is equivalent to the fraction of Xe in that trap site. This involves two components, the formation energy of the trap site (e.g. formation energy of vacancies) and the incorporation energy (the energy associated with adding Xe to the trap site). The sum of these two components is labeled the solution energy. The trap site with the lowest solution energy is the preferred location for Xe in the lattice. The trap site formation energy, and thus also the solution energy, is a function of $U_3Si_2$ stoichiometry or non-stoichiometry. Here we will assume that $U_3Si_2$ is perfectly stoichiometric. Expressions for the trap site formation energies in stoichiometric $U_3Si_2$ are listed in Table 3. Future work will consider non-stoichiometry and how that impacts the Xe solution energies. The concentration of Xe in trap sites is controlled by the free energy, G=H-TS, where G is Gibbs' free energy, H the enthalpy and S the entropy, however our initial analysis is restricted to enthalpies only. The enthalpy is equal to the internal energy for zero pressure conditions. Enthalpies provide a useful measure of the defect energies and are much easier to calculate than the corresponding entropies. Estimates of the entropies are also listed in Table 3, however they were not calculated and are only provided in order to enable calculation of approximate diffusivities. Calculation of entropies will be addressed in future work. Table 4 lists the calculated trap site formation, incorporation and solution energies. The preferred trap site for Xe is U vacancies of type 1 (see Figure 1) , but the U vacancy of type 2 and Si vacancies are only higher by a few tenths of an eV.

**Table 3: Expressions for the effective formation energy of Xe trap sites in stoichiometric $U_3Si_2$ as well as the resulting formation energy. The corresponding entropies have not been calculated (labeled by *), rather the listed values refer to estimates used to calculate diffusivities.**

| Trap site | Formula | Energy (eV) | Entropy ($k_B$) |
|---|---|---|---|
| U vacancy | $\Delta G_f=\Delta G_{Frenkel}/2$ | 1.14 | 5* |
| Si vacancy | $\Delta G_f=\Delta G_{Frenkel}/2$ | 1.14 | 5* |

**Table 4: Calculated Xe trap site formation, incorporation and solution energies.**

| Trap site | Trap site formation | Xe incorporation energy | Xe solution energy |
|---|---|---|---|
| Xe in U vacancy 1 | 1.14 | 3.15 | 4.30 |
| Xe in U vacancy 2 | 1.65 | 3.39 | 4.54 |
| Xe in Si vacancy | 1.14 | 3.39 | 4.53 |
| Xe in interstitial site | 0.00 | 6.07 | 6.07 |

## Migration of point defects

We have calculated the migration energies for U and Si interstitial and vacancies. There are a couple of different vacancy mechanisms because of the symmetry of the $U_3Si_2$ crystal structure, in particular diffusion may occur along the c axis or in the a-b plane. Some of the a-b plane mechanisms may also have a c component. For U there are two different crystallographic sites, giving rise to several different diffusion pathways. The main mechanisms are illustrated in Figures 4, 5 and 6. The results are shown in Table 5. Note that we only show results for mechanisms that give rise to

net diffusion, which implies that partial steps are not disclosed. Migration along the c axis is much faster than in the in-plane a-b mechanisms.

**Table 5: U and Si defect migration barriers. The notation a-b plane indicates that the main component of the migration distance is in the a-b plane. The notation c axis indicates that diffusion occurs along the c axis.**

| Defect | Migration barrier (eV) |
|---|---|
| U vacancy 1 (a-b plane) | 1.48 |
| U vacancy 1 (c axis) | 0.97 |
| U vacancy 2 (c axis) | 3.79 |
| U interstitial (a-b plane) | 0.54 |
| Si vacancy (a-b plane) | 2.24 |
| Si vacancy (c axis) | 0.64 |
| Si interstitial (a-b plane) | 3.05 |

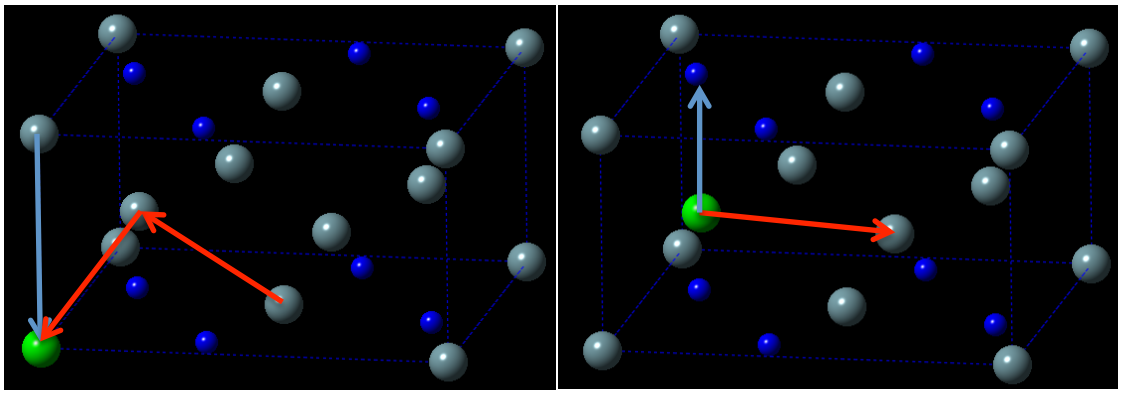

**Figure 4: The migration pathways for U vacancies in the first U lattice position (left). a-b plane migration is shown in red arrows and c –axis migration in a blue arrow. The migration pathways for U vacancies in the second U lattice position (a-b plane in a red and c –axis in a blue arrow).**

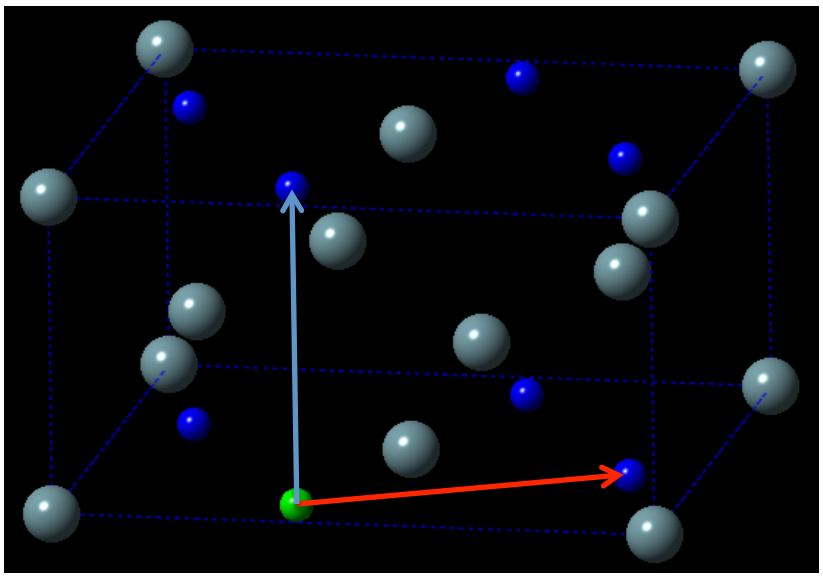

**Figure 5: The migration pathways for Si vacancies in the a-b plane (red arrow) and along the c –axis (blue arrow).**

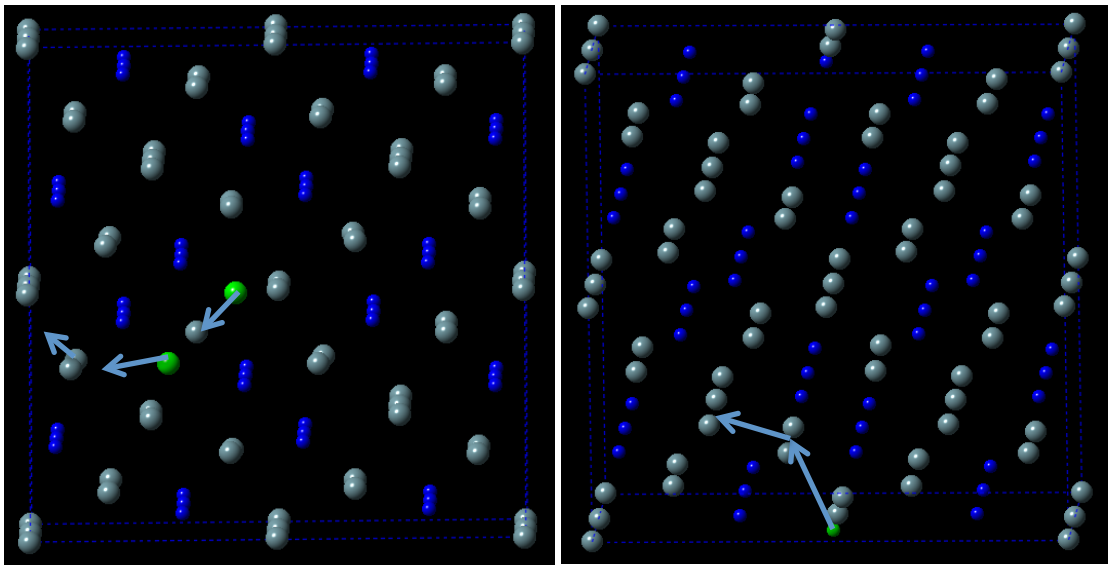

Figure 6: The migration pathway for the U split interstitial (left) and for a Si interstitial (right).

## Migration of Xe

Diffusion of Xe involves migration of Xe from one lattice site to another, which is governed by the concentration of mobile clusters, i.e. the concentration of vacancies bound to the Xe trap site for vacancy mechanisms, and the migration barrier for the rate limiting diffusion step of the cluster. We have investigated both interstitial and vacancy Xe diffusion mechanisms. The complex crystal structure of $U_3Si_2$ makes the diffusion mechanisms somewhat complicated. Diffusion may occur along the c direction (see Figure 7) or in the a-b plane (see Figure 8). We have calculated both rates for the interstitial and vacancy mechanisms. Three-dimensional Xe transport requires diffusion both in the a-b plane and along the c axis, which implies that it will be governed by the slowest rate of the two. However, it is possible that fission gas release may occur solely by diffusion along the c axis are or in the a-b plane. The interstitial diffusion mechanisms are illustrated in Figures 14 and 15 and the main vacancy diffusion mechanisms in Figures 7 to 13. For the vacancy mechanisms, the concentration of vacancies available at the trap site must be calculated. This is expressed by the vacancy formation energy and the binding energy of the vacancy to the Xe trap site. The formation, binding and migration energies are summarized in Table 6. As for point defects we only show results for mechanisms that give rise to net diffusion and partial steps are not disclosed. The formation energy of Xe interstitial is defined with respect to the most stable Xe vacancy trap site. As for point defect diffusion, Xe migration along the c axis occurs much easier than within the a-b plane.

Table 6: Formation, binding and migration energies for Xe diffusion mechanisms in $U_3Si_2$.

| Defect | Formation energy (eV) | Binding energy (eV) | Migration energy (eV) |
|---|---|---|---|
| Xe in a U vacancy 1 to another U vacancy 1 (c- | 1.14 | -0.54 | 1.08 |

| | | | |
|---|---|---|---|
| axis) | | | |
| Xe in a U vacancy 1 to another U 1 site via U vacancy 2 (a-b plane) | 1.65 | 0.099 | 2.81 |
| Xe in a U vacancy 1 to another U 1 site via a Si vacancy | 1.14 | 0.033 | 3.33 |
| Xe in a U vacancy 2 to another U 2 site via a Si vacancy | 1.14 | -1.59 | 8.68 |
| Xe in a Si vacancy to another Si vacancy (a-b plane) | 1.14 | 0.064 | 3.55 |
| Xe in a Si vacancy to another Si vacancy (c plane) | 1.14 | 0.18 | 1.09 |
| Xe in a Si vacancy to another Si site via a U vacancy 2 | 1.65 | -1.60 | 4.70 |
| Xe split interstitial, exchange with neighboring U atom (a-b plane) | 1.84 | N/A | 2.29 |
| Xe split interstitial, migration to another a-b plane along the c axis | 1.84 | N/A | 2.29 |

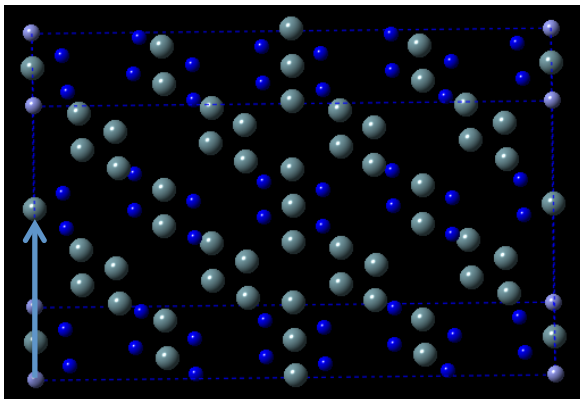

**Figure 7: Xe in a U vacancy 1 to another U vacancy 1 (c-axis).**

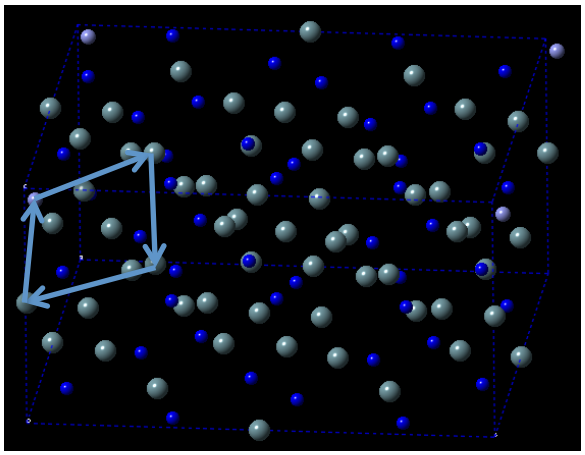

Figure 8: Xe in a U vacancy 1 to another U 1 site via a U vacancy 2 (a-b plane).

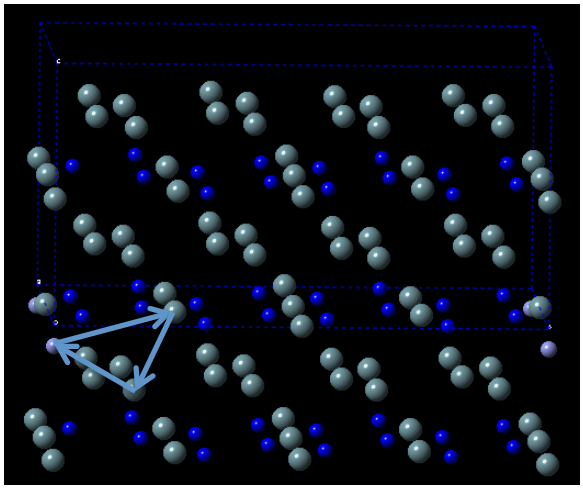

Figure 9: Xe in a U vacancy 1 to another U 1 site via a Si vacancy.

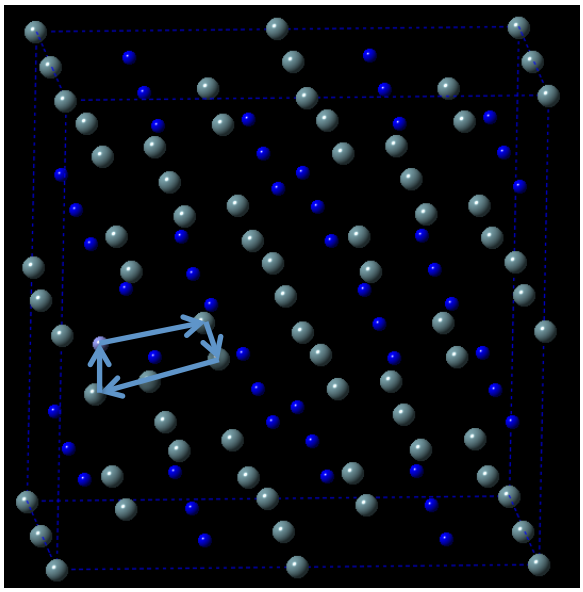

Figure 10: Xe in a U vacancy 2 to another U 2 site via a Si vacancy.

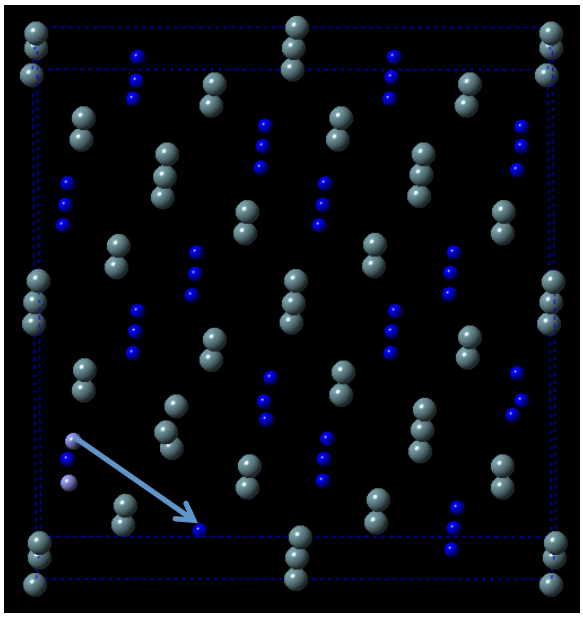

Figure 11: Xe in a Si vacancy to another Si vacancy (a-b plane).

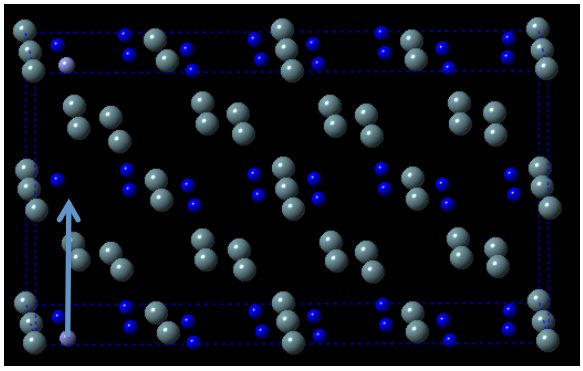

Figure 12: Xe in a Si vacancy to another Si vacancy (c plane).

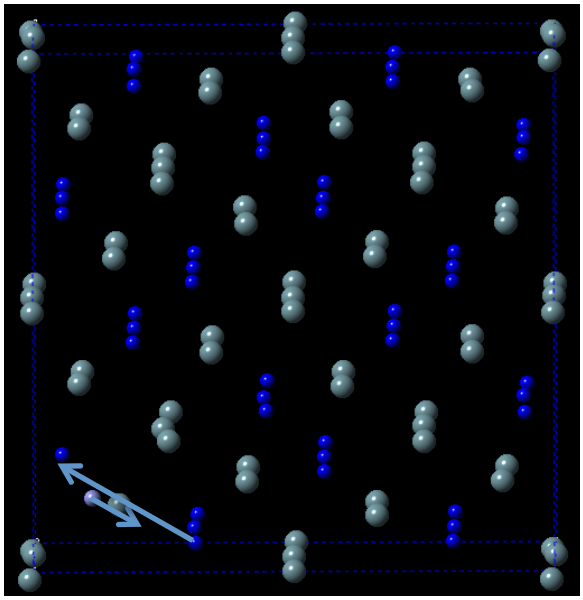

Figure 13: Xe in a Si vacancy to another Si site via a U vacancy 2.

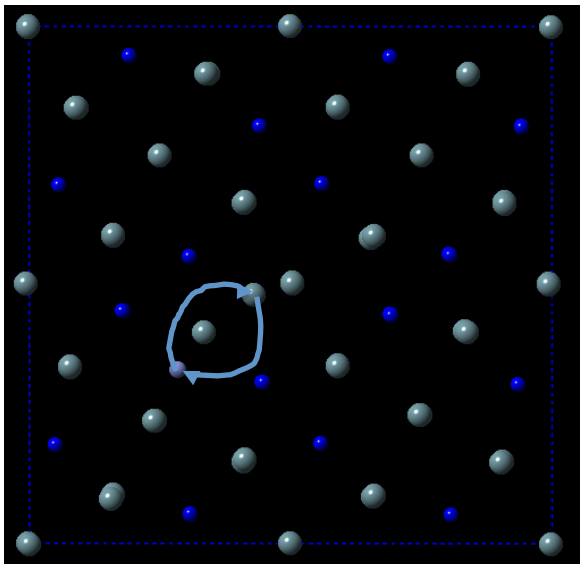

Figure 14: Xe split interstitial, exchange with neighboring U atom (a-b plane).

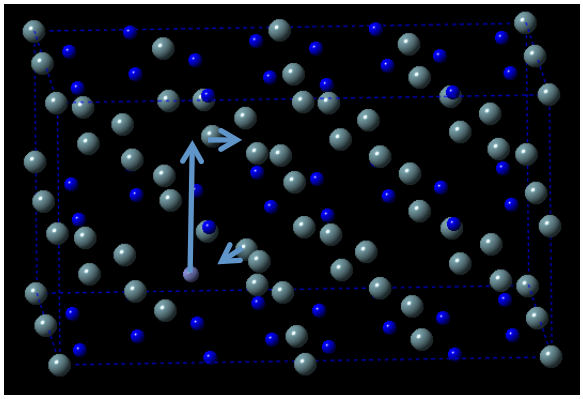

Figure 15: Xe split interstitial, migration to another a-b plane along the c axis.

## Point defect diffusion and self-diffusion

In order to calculate the diffusion rates of vacancies, interstitials as well as self-diffusion rates of U and Si we must make a few assumptions regarding the Frenkel (see Table 3) and binding entropies (assumed to be -1 $k_B$) as well as attempt frequencies for migration ($\upsilon_0$=$10^{13}$/s). The diffusivities are calculated as:

$$D = \frac{1}{6} fZS^2 \upsilon_0 \exp\left(\frac{\Delta G_a}{k_B T}\right) = D_0 \exp\left(\frac{\Delta H_a}{k_B T}\right)$$

where

$$\Delta G_a = \Delta G_f + \Delta G_m ,$$

$\Delta G_f$ is the defect formation energy and $\Delta G_m$ is the migration energy. f is the correlation factor (here assumed to be 1) and Z is the number of equivalent sites available for the migration jump. Note that the diffusivity for vacancies and interstitials does not involve any formation energy, while the corresponding self-diffusivities do. The resulting pre-exponential factors and activation energies are

listed in Table 7 and the diffusivities are plotted in Figure 16 and 17. U vacancies diffuse much faster along the c axis than within the a-b plane.

**Table 7: Activation energies and pre-exponential factors for defect and self-diffusion in $U_3Si_2$.**

| Diffusivity | $\Delta H_a$ (eV) | $D_0$ ($m^2/s$) |
|---|---|---|
| U vacancy (a-b plane) | 1.48 | $1.86\times10^{-6}$ |
| U vacancy (c-axis) | 0.97 | $5.27\times10^{-7}$ |
| U interstitial (a-b plane) | 0.54 | $1.30\times10^{-6}$ |
| U self-diffusion vacancy (a-b plane) | 2.63 | $2.17\times10^{-5}$ |
| U self-diffusion vacancy (c axis) | 2.12 | $2.26\times10^{-5}$ |
| U self-diffusion interstitial (a-b plane) | 1.68 | $1.58\times10^{-5}$ |
| Si vacancy (a-b plane) | 2.24 | $1.19\times10^{-6}$ |
| Si vacancy (c axis) | 0.64 | $5.30\times10^{-7}$ |
| Si interstitial (a-b plane) | 3.05 | $1.86\times10^{-6}$ |
| Si vacancy self-diffusion (a-b plane) | 3.38 | $1.45\times10^{-5}$ |
| Si vacancy self-diffusion (c axis) | 1.78 | $6.46\times10^{-6}$ |
| Si interstitial self-diffusion (a-b plane) | 4.19 | $2.27\times10^{-5}$ |

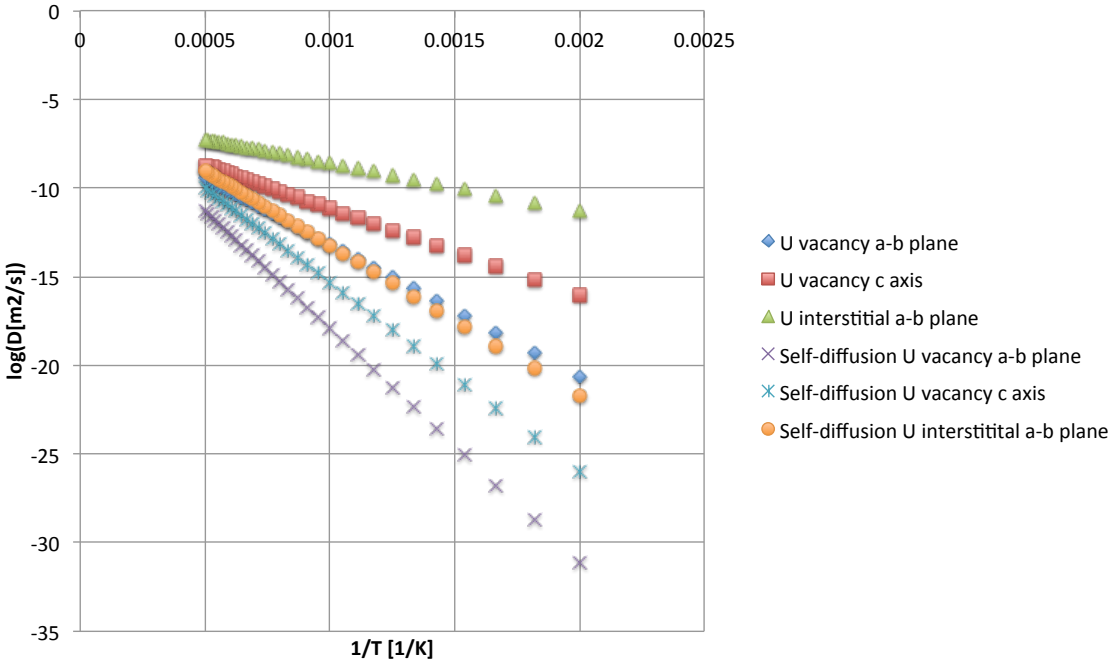


**Figure 16: Uranium vacancy and uranium interstitial diffusivities as well as the corresponding self-diffusion coefficients. The latter include the vacancy and interstitial formation energies.**

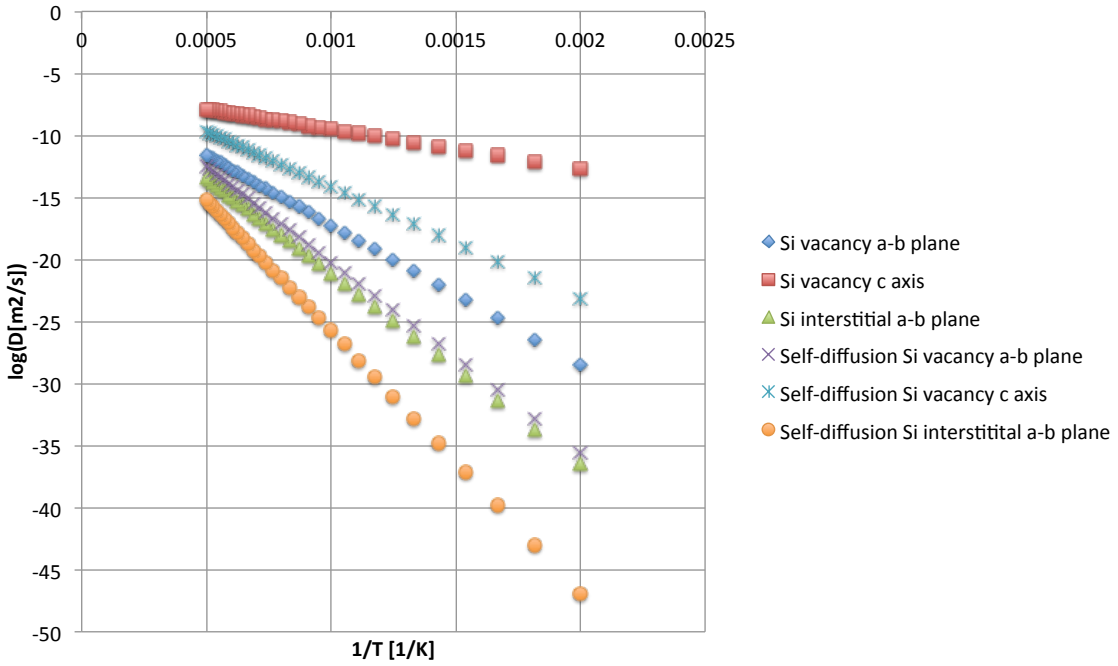


**Figure 17: Silicon vacancy and silicon interstitial diffusivities as well as the corresponding self-diffusion coefficients. The latter include the vacancy and interstitial formation energies.**

## Xe diffusion

Calculation of Xe diffusivities involves the same assumptions for the Frenkel and Schottky formation entropies as for the point defect diffusivities. The Xe diffusivities are calculated as:

$$D = \frac{1}{6} fZS^2 \upsilon_0 \exp\left(\frac{\Delta G_a}{k_B T}\right) = D_0 \exp\left(\frac{\Delta H_a}{k_B T}\right)$$

where

$$\Delta G_a = \Delta G_f + \Delta G_b + \Delta G_m$$

$\Delta G_f$ is the defect formation energy, $\Delta G_b$ the binding energy and $\Delta G_m$ is the migration energy. f is the correlation factor (here assumed to be 1) and Z is the number of equivalent sites available for the migration jump. Note that the diffusivities for interstitial mechanisms do not involve any binding energy, while the corresponding vacancy mechanisms do. Except for mechanisms that involve the most stable Xe trap site, there is an extra contribution to the activation energy from the energy difference between the lowest energy trap site and the trap site involved in the diffusion mechanism. The resulting pre-exponential factors and activation energies are listed in Table 8 and the diffusivities are plotted in Figure 18 and 19. The intrinsic and radiation-enhanced diffusion coefficients for $UO_2$ are also included for comparison. Xe atoms diffuse much faster along the c axis than within the a-b plane. Diffusion along the c axis is faster than in $UO_2$, while in-plane diffusion is slightly slower. The difference between Figures 18 and 19 is that in the latter the formation and binding energies are not included in the activation energy, which only comprises the migration energy and corresponds to cluster diffusion. The cluster

diffusivities represent an upper bound for Xe gas diffusion that is valid for high concentration of irradiation-induced vacancies.

**Table 8: Activation energies and pre-exponential factors for Xe diffusion in $U_3Si_2$ according to different mechanisms.**

| Diffusivity | $\Delta H_a$ (eV) | $D_0$ ($m^2/s$) |
|---|---|---|
| Xe in a U vacancy 1 to another U vacancy 1 (c-axis) | 1.68 | $2.32\times10^{-6}$ |
| Xe in a U vacancy 1 to another U 1 site via U vacancy 2 (a-b plane) | 4.56 | $8.28\times10^{-6}$ |
| Xe in a U vacancy 1 to another U 1 site via a Si vacancy | 4.50 | $8.28\times10^{-6}$ |
| Xe in a U vacancy 2 to another U 2 site via a Si vacancy | 8.47 | $5.43\times10^{-6}$ |
| Xe in a Si vacancy to another Si vacancy (c plane) | 3.79 | $2.29\times10^{-6}$ |
| Xe in a Si vacancy to another Si vacancy (a-b plane) | 4.98 | $1.02\times10^{-5}$ |
| Xe in a Si vacancy to another Si site via a U vacancy 2 | 4.98 | $9.96\times10^{-6}$ |
| Xe split interstitial, exchange with neighboring U atom (a-b plane) | 5.90 | $6.96\times10^{-7}$ |
| Xe split interstitial, migration to another a-b plane along the c axis | 5.90 | $2.46\times10^{-6}$ |

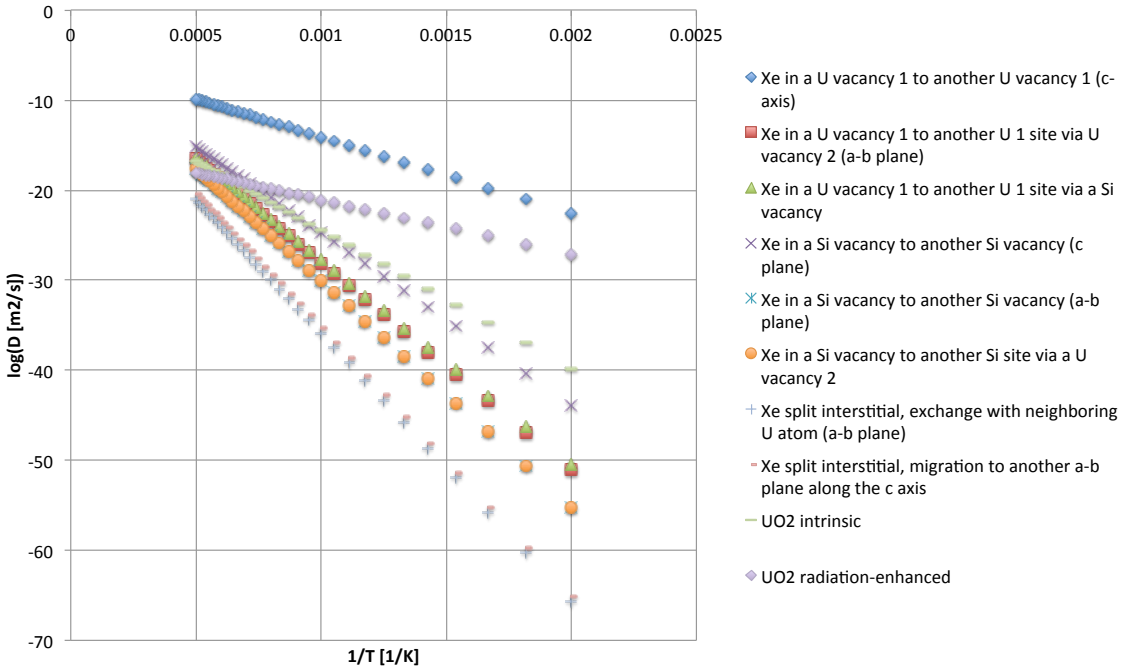


**Figure 18: Calculated intrinsic Xe diffusivities for different mechanisms in $U_3Si_2$. The intrinsic and radiation-enhanced diffusion coefficients for $UO_2$ are also included for comparison.**

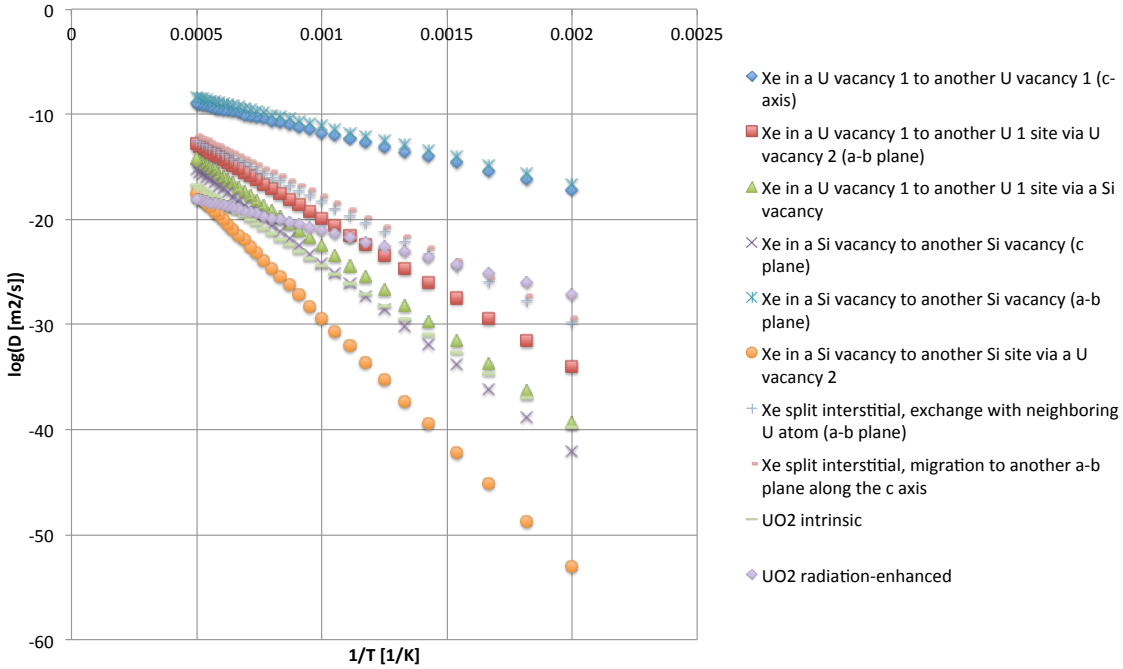


**Figure 19: Calculated Xe cluster diffusivities for different mechanisms in $U_3Si_2$. Unlike Figure 18, the formation and binding energies are not included in the activation energy, which only comprises the migration energy. The intrinsic and irradiation-enhanced diffusion coefficients for $UO_2$ are also included for comparison.**

## Conclusions

We have investigated point defect and fission gas properties in $U_3Si_2$, which is one of the main accident tolerant fuel (ATF) candidates, using density functional theory

(DFT) calculations. The regular GGA (PBE) approach to describe the exchange-correlation effects predicts the $U_3Si_2$ structure to develop significant structural distortions, though there is no experimental support for this result. However, applying the Hubbard *U* method to capture the strongly correlated nature of the U 5f electrons recovers the experimental structure as the most stable. We used the Hubbard *U* method to calculate the preferred Xe trap site (U vacancies, closely followed by Si vacancies) and Xe diffusivities. Xe atoms diffuse much faster along the c axis than within the a-b plane of the $U_3Si_2$ structure. Diffusion along the c axis is faster than in $UO_2$, while in-plane diffusion is slightly slower. Point defect diffusion similarly exhibits high diffusivities along the c axis and low diffusivities within the a-b plane of the $U_3Si_2$ structure. The low symmetry of the $U_3Si_2$ implies that the diffusion mechanisms are fairly complex and involve multiple steps.

## References


[1] G. Kresse and J. Hafner, Phys. Rev. B **48**, 13115 (1993).
[2] G. Kresse and J. Furthmüller, Comput. Mater. Sci. **6**, 15 (1996).
[3] G. Kresse and J. Furthmüller, Phys. Rev. B **54**, 11169 (1996).
[5] G. Kresse and D. Joubert, Phys. Rev. B **59**, 1758 (1999).
[6] P.E. Blöchl, Phys. Rev. B **50**, 17953 (1994).
[7] J. P. Perdew, K. Burke and M. Ernzerhof, Phys. Rev. Lett. **77**, 3865 (1996).
[8] S.L. Dudarev, D.N. Manh, A.P. Sutton, Philos. Mag. **75**, 613 (1997).
[9] A. Jain, G. Hautier, S. P. Ong, C. J. Moore, C. C. Fischer, K. A. Persson and G. Ceder, Phys. Rev. B: Condens. Matter Mater. Phys. **84**, 045115 (2011).